Content available at: https://www.ipinnovative.com/open-access-journals

Indian Journal of Microbiology Research

Journal homepage: www.ijmronline.org

Original Research Article

Structural insight into Cot H3 protein inhibition targeting mucormycosis infection through computational approaches

Sugumaran Muthuraj[1], Nalina Viswanathan[1], Kavitha Thangavel[2], Prabhu Dhamodharan[3], Vidhyavathi Ramasamy[1*]

[1]Dept. of Bioinformatics, Alagappa University, Karaikudi, Tamil Nadu, India
[2]Dept. of Microbiology, Alagappa University, Karaikudi, Tamil Nadu, India
[3]Dept. of Biotechnology, Karpagam Academy of Higher Education, Coimbatore, Tamil Nadu, India

Abstract

Background: This study aims to identify potential antifungal phytocompounds targeting the spore coat protein COT H3 from *Rhizopus*, a critical virulence factor in mucormycosis. Mucormycosis, caused by *Rhizopus* species, is a rapidly progressing and often fatal fungal infection with limited treatment options. COT H3 plays a key role in immune evasion, making it an ideal target for antifungal therapy. The objective is to discover compounds that inhibit COT H3, offering a novel therapeutic strategy.

Materials and Methods: A comprehensive in-silico approach was employed, utilizing protein modeling, molecular docking, molecular dynamics (MD) simulations, and binding free energy calculations to screen antifungal phytocompounds. The top compound, Emodin was subjected to ADME (absorption, distribution, metabolism, and excretion) and toxicity analyses to evaluate its drug-like properties and safety.

Results: Emodin demonstrated the highest glide score (-8.37 kcal/mol) and binding free energy (-33.735 kcal/mol). Strong interactions were observed with key residues, including Thr573, Asn571, and Ser408. MD simulations confirmed the stability of the emodin-COT H3 complex. ADME and toxicity analyses showed favorable drug-like properties for emodin.

Conclusion: Emodin exhibits strong potential as an antifungal agent against mucormycosis by inhibiting COT H3. These findings highlight emodin as a promising lead for novel antifungal therapies, improving treatment options for this serious infection.

Keywords: *Rhizopus arrhizus*, Mucormycosis, Cot H3, COVID-19, Phyto-chemical compounds.

Received: 26-11-2024; **Accepted:** 27-02-2025; **Available Online**: 01-07-2025

1. Introduction

A peculiar fungal ailment known as "black fungus" affects one in 10,000 individuals and has a 50% death rate. Even with the terrible COVID-19 epidemic, there is yet more disease-causing devastation across the nation: "black fungus," popularly known as "mucormycosis".[1,2] One of the most researched orders of fungi, the Mucorales, is responsible for several fungal illnesses and mycoses, including mucormycosis.[3,4] According to estimates, Between 0.005 and 1.7 people per million are affected by mucormycosis. Even so, the incidence is up to 0.14 per 1000 persons in nations like India, which is over 80 times higher than the global average.[5]

The prevalence of mucormycosis has increased in recent decades, which may be related to a growth in the number of people with severe immunocompromised individuals.[6,7] A black fungus infection can be lethal in those with severely impaired immune systems, affecting the brain, lungs, and sinus cavities. Eyelid drooping, pleural effusion, deterioration of respiratory symptoms, blackish darkening around the nose, bleeding, stuffy nose, black crusts in the nose, weakened teeth, jaw difficulty, hemisphere discomfort or numbness, and bulging in the eyes are among the most common symptoms.[8,9]

*Corresponding author: Vidhyavathi Ramasamy
Email: vidhyavathirm@alagappauniversity.ac.in

https://doi.org/10.18231/j.ijmr.2025.039

Mucormycosis is well-known for its high death rates and correlation with angio-invasion.[4,5] Patients receiving corticosteroid medication, solid organ transplants, hematological malignancies, and diabetes mellitus are among the groups in whom the infection is becoming more common.[6,7] It is noteworthy that there are differences in the incidence of risk factors and causal agents for mucormycosis between Asian and Western nations.[8,9] Diabetes mellitus is the most prevalent risk factor in Asia, whereas hematological malignancies and transplantation are the main risk factors in Europe and the US.[10,11]

Furthermore, a sizable number of cases in otherwise healthy people have been documented after trauma. Moreover, mucormycosis linked to healthcare facilities has increased recently.[12] Many fungus from the order Mucorales, the most common of which are *Rhizopus oryzae* or *Rhizopus arrhizus*, cause the infection. Species of *Rhizopus*, the most common fungi in the Mucorales order, are responsible for about 70% of cases of mucormycosis. *Rhizopus arrhizus* is a type of fungus belonging to the Mucoraceae family.[13,14] It is distinguished by hemispherical columella and sporangiophores that emerge from nodes at the rhizoids' formation site. It is occasionally responsible for infecting other animals and is the most prevalent cause of mucormycosis in humans. Ribosomes are a component of the spore ultrastructure of *Rhizopus arrhizus* spores.[15,16]

Mucormycosis, stemming from the inhalation of filamentous fungi, particularly in the hyphal form, predominantly affects individuals with compromised immune systems.[17,18] The growth of hyphae around blood vessels characterises this infection, posing severe risks to immunocompromised patients. Virulence factors of the pathogen, notably the Mucorales spore coat (Cot H3) protein, particularly Cot H3, play a pivotal role in invading and disrupting immune cells.[19,20] Epithelial cells, the primary defense against fungal pathogens, are targeted by mucoralean fungi through enhanced growth factor receptor B (PDGFRB) signaling in platelets, fostering fungal growth. Neutrophils, crucial components of innate immunity, become less effective in diabetic or steroid-using patients due to conditions like ketoacidosis or hyperglycemia, allowing fungal hyphae to thrive.[21] Once inside the host cell, Mucorales produces Mucorales-specific T-cells, which release pro-inflammatory cytokines, further damaging the host cell. Additionally, fungal hyphae inhibit the production of immunomodulatory chemicals, impairing the host's immune response. These insights elucidate the susceptibility of immunocompromised individuals to mucormycosis and its mechanisms within the host cell.[22]

Phytochemical plants have gained significant attention in modern medicine as sources of therapeutic agents, driven by their natural abundance, effectiveness, and safety.[23] Changes in disease patterns, environmental conditions, and population growth drive this shift. The therapeutic efficacy of medicinal plants depends on the quality and quantity of their phytochemicals, making quality control essential. Over 50% of modern medicines originate from natural products, which are crucial in drug development. The rising prevalence of diseases, coupled with changing environmental conditions and increasing population demands, has prompted the allopathic world to explore plant-derived compounds for drug development.[24] The therapeutic potential of these medicinal plants is largely attributed to their phytochemicals—bioactive compounds that contribute to their medicinal properties.[25,26] As more than 50% of contemporary medicines are derived from natural sources, quality control of these plants is essential to ensure their efficacy and safety. Notable examples include *Ziziphus joazeiro, Cassia tora, Alphinia galanga, Syzygium aromaticum, Curcuma longa, Datura metel, Datura stramonium, Eugenia uniflora, Azadirachta indica, Origanum vulgare, Citrus lemon, Thymus vulgaris, Wrightia tinctoria and Zingiber officinale have all been reported as therapeutic plants for treating fungal infection around the globe*, which have demonstrated antifungal, antiviral, and antibacterial properties, highlighting their importance in treating infections on a global scale. This growing interest underscores the need for continued research and integration of phytochemical plants in modern therapeutic practices.[27] The study utilises computational methods, which include techniques like virtual screening, docking, and dynamics simulations, to explore how potential inhibitors can interact with the Cot H3 protein. These approaches allow for the analysis of protein-ligand interactions, prediction of binding sites, and identification of potential drug candidates without the immediate need for experimental work.[28]

2. Materials and Methods

2.1. Homology modelling and validation

The Cot H3 protein sequence (COTH3_RHI09) was sourced from UniProt. The Expasy ProtParam tool calculated its physical and chemical properties, including GRAVY, pI, atomic composition, molecular weight, instability index, and estimated half-life. The amino acid sequence for *R. arrhizus* (UniProt ID: I1CFE1) was modeled using Robetta Server, while its secondary structure was predicted with SOPMA. The 3D structure was validated using the SAVES 6.0 server and a Ramachandran plot.[14,15]

2.2. Molecular dynamics simulation of apoprotein and complex

Molecular dynamics simulations of the modeled apoprotein were performed using the GROMACS software and the Gromos 43a1 force field.[24] Energy minimization reduced steric clashes and strains while maintaining the protein structure. Root Mean Square Deviation (RMSD) and Root Mean Square Fluctuation (RMSF) were calculated for the minimised protein. At 50 ns, MD simulations modelled the Cot H3 protein-ligand complex, with trajectories separated

by two picoseconds. The RMSD, RMSF, salt bridge contacts, hydrophobic, and hydrogen bond interactions were analysed, and XM Grace software was used for graphical representation.[13]

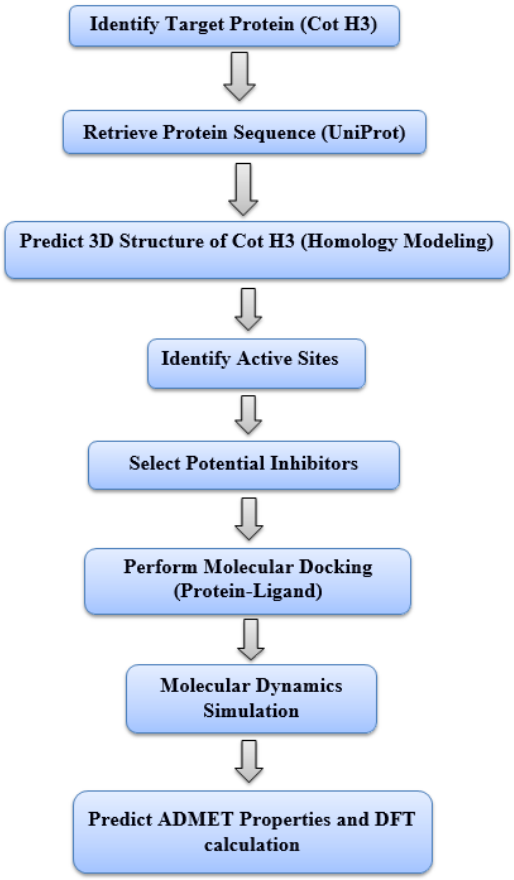

Figure 1: Methodology flow chart

2.3. Molecular docking

The Cot H3 protein was synthesised using Schrödinger's Protein Preparation Wizard, which involved preprocessing steps like loop filling, water removal, hydrogen addition, polar hydrogen display, and bond order assignment.[26] Optimisation included refining hydrogen bonds and clusters. The OPLS 2005 force field was applied to estimate partial atomic charges and optimise RMSD values. The PASS prediction algorithm selected 100 phyto-compounds from 14 medicinal plant families for ligand preparation. Schrödinger's LigPrep module generated these ligands, sourced from PubChem. Ligand preparation included hydrogen addition, bond order correction, and ionization at pH 7.0 ± 2 using Epik. Conformational sampling produced up to 32 conformations per ligand. Five binding sites were identified using Sitemap, and the optimal site was selected for docking with Schrödinger's GLIDE module.[27,31]

2.4. ADME/T properties prediction:

The absorption, distribution, metabolism, and excretion (ADME) characteristics of target compounds were studied using Schrödinger's QikProp version 4.3. This tool predicted key properties of selected ligands, including log P, oral absorption, and Lipinski's rule of five, which are vital for drug design. The study examined 100 antifungal drugs with ADME properties. BOSS software and the OPLS-2005 force field were used to model organic solutes within a water molecule periodic box.[11] The toxicity risk of compounds was evaluated, assessing reproduction toxicity, irritability, tumorigenicity, and mutagenicity. The lead compound from Glide XP was selected for toxicity prediction using the Property Tox Checker and ProTox, which predicts harmful properties based on functional group similarity to in vitro and in vivo data.[2]

2.5. Prime MMGBSA

Solvent accessibility and ligand binding of the collection of phytochemicals attached to receptors were examined using Solvent Accessibility and the Generalized Born Model in Prime Molecular Mechanics (MM-GBSA). Prime MM-GBSA uses the OPLS-AA, SGB solvation model for polar solvation, Molecular Mechanics Energies, and nonpolar solvation (which covers numerous nonpolar SASA and van der Waals interactions.[27]

2.6. DFT calculation

The primary study of molecules was done on the theory of density functions (DFT) obtained from the ligand docking studies. DFT was applied to the lead complex Emodin (3220). LUMO, HOMO, and electron density are the three main features that DFT computes to predict the lead molecule's chemical characteristics and biological activities [9][31]. Hybrid DFT helps collect precise geometric details of the molecule. Among other molecular electrostatic parameters, the Jaguar v8.7 module was used to calculate the highest occupied molecular orbital (HOMO), the dipole moment, the unoccupied molecular orbital (LUMO), and MESP. Colour distinctions were used to identify different regions within the compounds, and the compounds of interest's electrostatic potential was assessed as either positive or negative.[28]

3. Results

3.1. Physico-chemical characteristics

The physicochemical properties of the Cot H3 protein, including its aliphatic index, GRAVY (Grand Average of Hydropathicity), isoelectric point (pI), instability index, and molecular weight, were predicted and summarised. Cot H3 has a molecular weight of 65,759.18 Daltons and a projected pI of 5.7, indicating its acidic nature due to a higher proportion of negatively charged amino acids (57%) compared to positively charged ones (43%). The protein's instability index was 29.46, classifying Cot H3 as stable. Its GRAVY value of -0.284 indicates the protein is hydrophilic and soluble. The extinction coefficient at 280 nm was 103,250 M^{-1} cm^{-1}. The aliphatic index, indicating thermo stability, was 73.11, suggesting Cot H3 may remain stable across a wide range of temperatures.[33]

3.2 Secondary structure prediction:

SOPMA predicted the beta-turn, random coil, prolonged strand, and alpha helix from the protein's secondary structure chains. Alpha helices were visible in the Cot H3 protein's planned secondary structure at 29.45% (177 residues), random coil showed 52.08% (313 residues), beta-turn showed 2.16% (13 residues), and followed by extended strands showed 16.31% (98 residues) **(Table 1)**. The prominent form of helix and coiling was identified in the Cot H3 proteins, emphasizing the Cot H3 protein's more compact and tightly correlated transmembrane region. **(Figure 2).**[34,35]

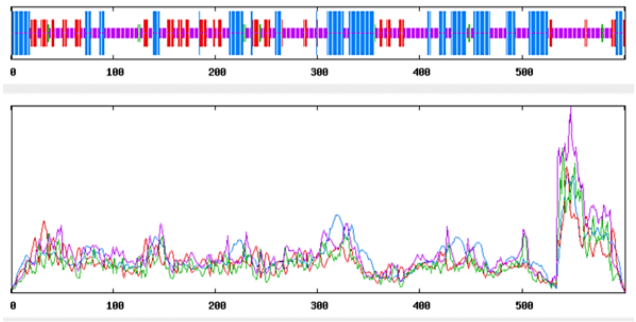

Figure 2: SOPMA- Secondary structure prediction of Cot H3

Table 1: Secondary structure prediction of Cot H3 protein

Parameters	Percentage (%)
Alpha helices	29.45
Random coils	52.08
Beta turn	2.16
Extended strands	16.31

3.3. Validation of homology modeling

The Cot H3 protein model was built using ROBETTA's automated protein modeling system in the absence of experimental structural data **(Figure 3)**. The Ramachandran plot, validated by the ProCheck tool, showed that 90.8% of the residues were in the generously allowed regions, with 0.2% in disallowed regions and 8.6% in the core area. The model was deemed high-quality, as over 90% of residues were in preferred locations on the Ramachandran plot.[37]

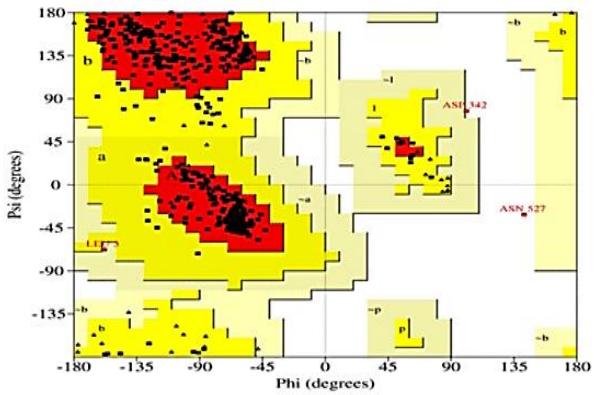

Figure 3: Modeled Cot H3 protein Ramachandran plot

3.4. Molecular dynamic simulation of apoprotein

The MD simulation reveals structural stability and dynamic patterns in the Cot H3 model. RMSD and RMSF are key measures of model stability. RMSD quantifies the average displacement of backbone atoms from the reference structure over time, calculated from the protein's initial configuration. During the 50-ns simulation, the RMSD value remained stable at 1.5 nm, indicating protein stability **(Figure 4)**. The protein's residual variations during dynamic behaviour are shown in **(Figure 4)**, further confirming the stability of the model.[37]

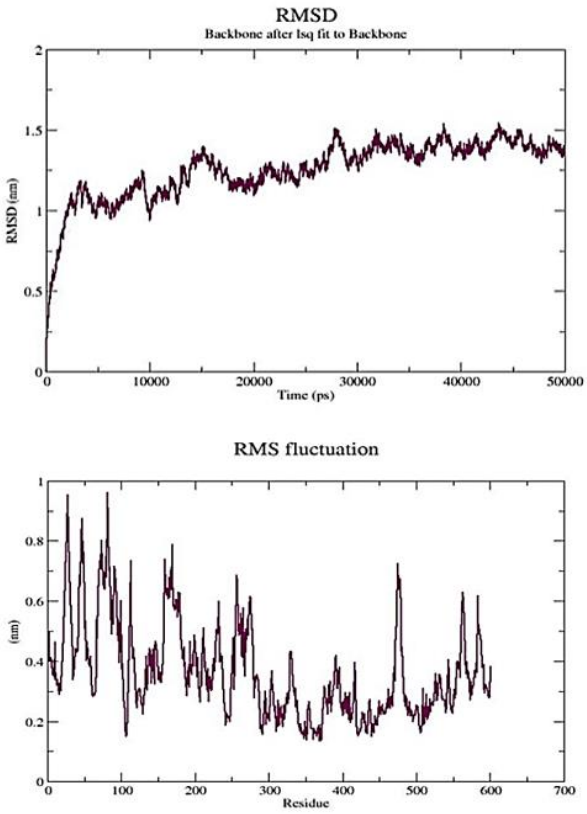

Figure 4: RMSD and RMSF fluctuation for the apoprotein observed during the simulation time

3.5. Ligand selection and bioactivity prediction

The bioactivity of phytochemical compounds was predicted using the PASS prediction tool, which computes probabilities (Pa > Pi) for potential activities, mechanisms of action, and pharmacological effects. Pa and Pi values range from 0.000 to 1.000, with Pa > 0.7 indicating a high likelihood of activity. Compounds with 0.5 < Pa < 0.7 may be harder to identify experimentally, while Pa < 0.5 suggests novelty and a low probability of showing the predicted activity. Compounds with Pa ≥ 0.7 were selected for further experimental investigation, prioritizing high-Pa compounds while considering lower-Pa compounds for novel discoveries **(Figure 5)**.

3.6 Active site prediction

Understanding the protein's function is essential for improving our understanding of structure-based drug design, and here is where the protein-ligand complex comes in. SiteMap ranks the predicted binding sites according to their druggability and SiteScore. Site and druggability scores for the highest-ranking site were 1.03 and 1.05, respectively **(Figure 5).** Aminoacid residues such as 354, 355, 362, 363, 384, 386, 388, 389, 399, 400, 401, 402, 404, 406, 407, 408, 409, 410, 411, 412, 432, 435, 436, 439, 440, 443, 534, 535, 536,537, 538, 539, 540, 541, 543, 545, 547, 548, 549, 554, 556, 568, 570, 571, 572, 573, 574, are anticipated to be functional for molecular docking investigations.[33,34]

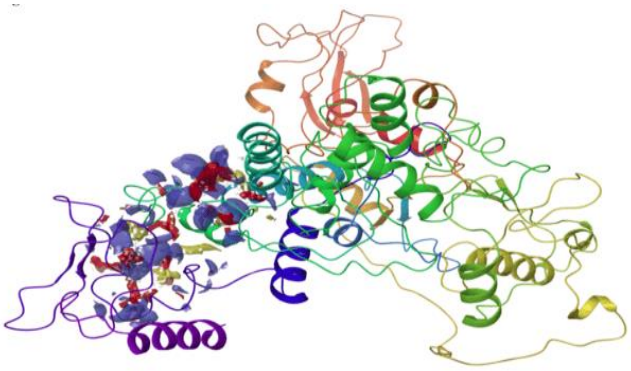

Figure 5: Binding site prediction using Site Map in Schrondinger

3.7. Ligand docking

The Cot H3 protein was refined using a wizard tool, and its active site, critical for docking studies, was identified using the "map" tool, which located the binding regions. The Glide grid-generating tool defined the active region, creating a grid box around the receptor's active site. LigPrep generated 100 phytochemical compounds, which were docked into the protein's active site. Five compounds showed the strongest binding affinities based on docking scores: Compound 3220 (-8.371 kcal/mol), Compound 328441 (-8.261 kcal/mol), Compound 44259428 (-7.925 kcal/mol), Compound 12311099 (-7.849 kcal/mol), and Compound 5281673 (-6.535 kcal/mol). Hydrogen bond interactions were observed at residues SER 408, THR 573, ASN 571, and others, while PHE 412 exhibited Pi-Pi stacking. **Figure 6** and **Figure 7** show the docked compounds' positions, and **Table 2** details the interaction analysis of the lead compounds.

Table 2: Docking score for the phytochemical compounds against Cot H3 protein

Pubchem Id	Compound Name	Docking Score (Kcal/Mol)	Xp Score	Interacting Residues	Bond Length	Bond Type
3220	Emodin	-8.371	-8.464	SER 408	1.79	Hydrogen bond
				THR 573	2.14	
				ASN 571	1.89	
328441	Diosgenin tetra glycoside	-8.261	-8.261	ASP 411	2.04	Hydrogen bond
				ASP 406	1.95	
				THR 573	2.05	
				LYS 410	2.73, 2.04, 2.01,1.91	
44259428	Myricetin-3-O-rutinoside	-7.925	-9.850	ASP 385	1.94, 1.84	Hydrogen bond Pi-Pi stacking
				TYR 409	2.00	
				GLU 400	1.74	
				PHE 412	5.37, 5.21	
12311099	Myricetin-3-O-hexoside	-7.849	-9.775	GLU 400	1.80, 1.61	Hydrogen bond
				PRO 534	2.13	
				ASP 385	1.95	
				ASP 389	1.81	
				TYR 409	1.80	
				SER 408	2.04	
5281673	Myricitrin	-6.535	-7.121	GLU 400	1.82, 1.58	Hydrogen bond
				PRO 534	2.23	
				ASP 389	2.13	
				TYR 409	1.90	
				SER 408	1.87	

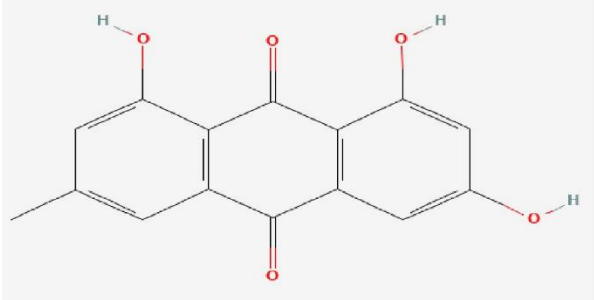

3220

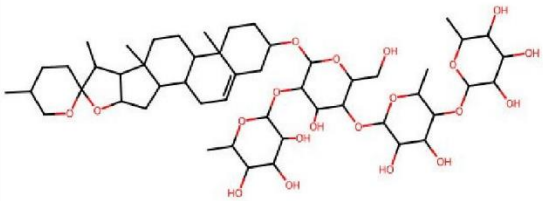

328441

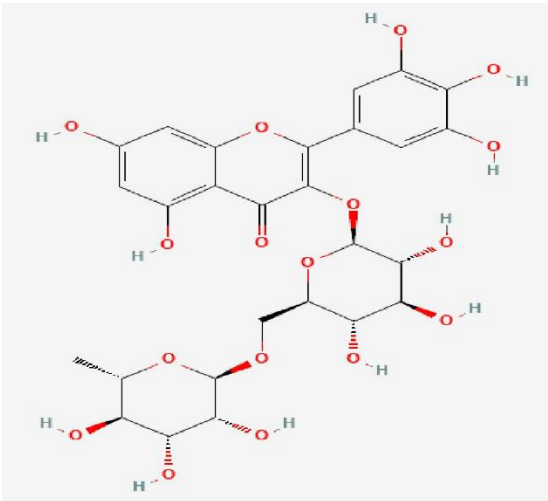

44259428

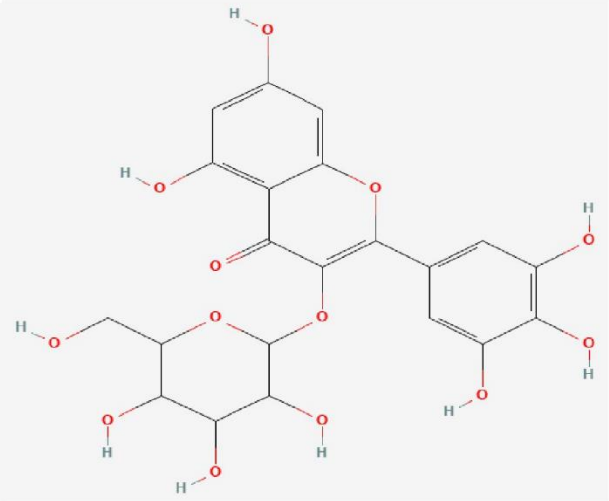

12311099

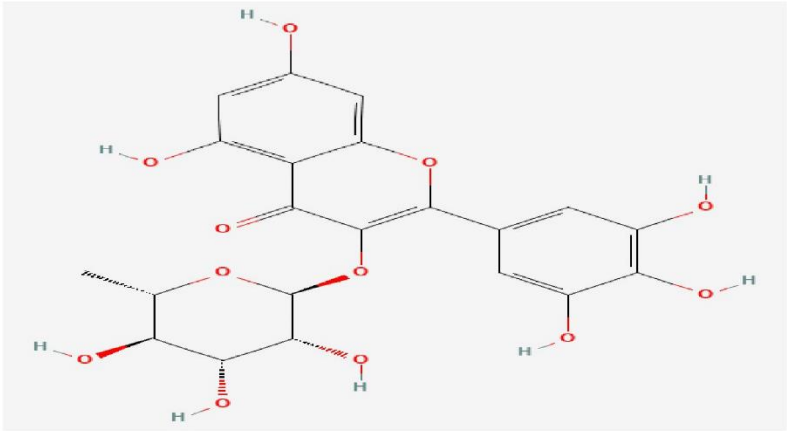

5281673

Figure 6: Chemical structures of the five Lead molecules

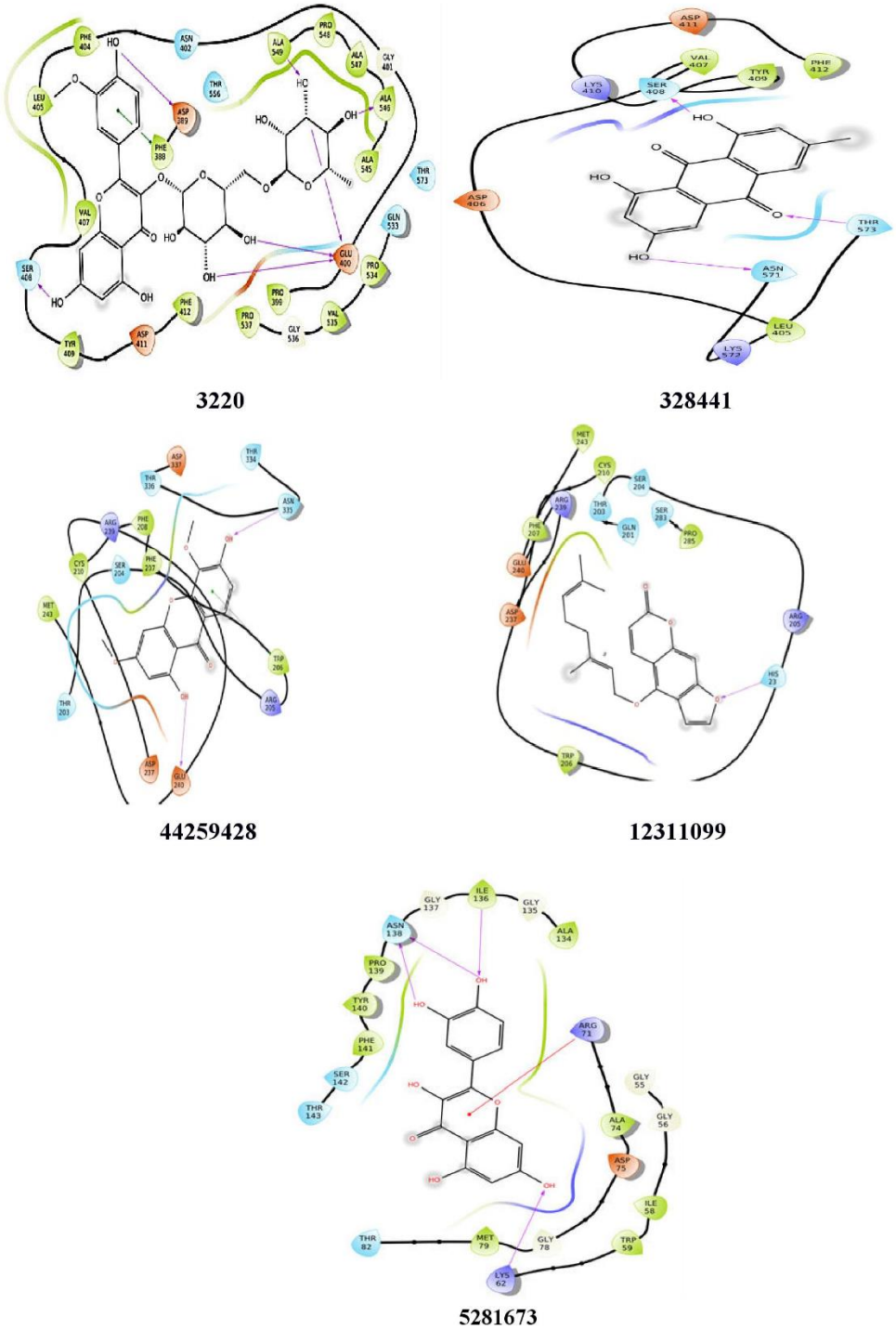

Figure 7: 2D interaction between lead compounds and Cot H3 Protein

3.8. Binding free energy calculation

Based on the docking complex, the primary / MM-GBSA approach calculates the ligand binding free energy (Gbind). Gbind, the PRIME MM/GBSA of the top five lead compounds, 3220 (compound1) have -33.735 kcal/mol, 328441 (compound2) have -41.643 kcal/mol, 44259428 (compound 3) have -57.305 kcal/mol, 12311099 (compound 4) have -48.229 kcal/mol and 5281673 (compound 5) have -48.843 kcal/mol respectively **(Table 3)**.

Table 3: Glide score, glide energy, glide e model of the of the lead compounds docked with Cot H3 protein

Compound	Docking score	XP Score (kcal/mol)	Glide energy (kcal/mol)	Glide e model
Compound 1	-8.371	-8.464	-33.735	-45.037
Compound 2	-8.261	-8.261	-41.643	-66.780
Compound 3	-7.925	-9.850	-57.305	-76.576
Compound 4	-7.849	-9.775	-48.229	-66.780
Compound 5	-6.535	-7.121	-48.843	-64.091

Table 4: ADME properties for lead compound

Compound	MW	HOA (%)	HB acceptor	HB donor	Qplog Po/w	QPlogHERG	QPPcaco	QPPMDCK	Rule of five
3220	270	68	4.25	1	1.259	-4.357	79.596	32.088	0

Table 5: ADME properties for drug compound

Compound	MW	HOA (%)	HB acceptor	HB donor	Qplog Po/w	QPlogHERG	QPPcaco	QPPMDCK	Rule of five
5280965	924	0	23	11	-0.380	-5.022	0.024	0.007	3

MW: Molecular Weight; HOA (%): Human Oral Absorption (percentage); HB acceptor: Hydrogen Bond Acceptor; HB donor: Hydrogen Bond Donor; Qplog Po/w: Predicted Logarithm of the Partition Coefficient between Octanol and Water; QPlogHERG: Predicted Logarithm of IC50 value for blocking the HERG K+ channel (an indicator of potential cardiac toxicity); QPPcaco: Predicted Caco-2 Cell Permeability (used to estimate intestinal absorption); QPPMDCK: Predicted MDCK Cell Permeability (used to assess blood-brain barrier penetration)

Table 6: Toxicity of the lead compound predicted by Property tox checker

S. No.	Compound	Predicted LD50(mg/kg)	Hepatotoxicity	Carcinogenicity	Immunotoxicity	Cytotoxicity
1	3220	5000	Inactive	Inactive	Inactive	Inactive

Table 7: Toxicity of the drug compound predicted by Property tox checker

S. No.	Compound	Predicted LD50(mg/kg)	Hepatotoxicity	Carcinogenicity	Immunotoxicity	Cytotoxicity
1	5280965	5000	Active (mild)	Inactive(mild)	Active	Inactive

3.9. ADME prediction

ADME prediction was performed on 100 phytochemical compounds to assess their pharmacokinetic activity. Key parameters, such as molecular weight, Lipinski's rule violations, human oral absorption, aqueous solubility, and octanol/water partition coefficient, were analysed **(Table 4)**. Among the top five lead compounds, only Emodin (PubChem ID: 3220) complied with ADME parameters **(Table 5)**. Notably, compound 3220 was identified as a lead compound across all five proteins.[28]

3.10. Toxicity prediction

In silico toxicity, prediction is crucial for assessing compounds before experimental testing. The lead compound showed minimal toxicity, with an estimated LD50 of 5000 mg/kg, indicating it is mostly benign, as predicted by the ProTox-II toxicity service **(Table 6).** Compared to synthesized drugs, the lead compound demonstrated superior results, as one drug with an LD50 of 100 mg/kg indicated toxicity **(Table 7).**[31]

3.11 Molecular dynamics simulations of complexes

A 50 ns time scale was used to simulate each complex, and Gromacs trajectory files were analysed to evaluate the RMSD of the backbone atoms and stability of the docked complexes.[39] The RMSD results showed no significant divergence between the natural protein and protein-ligand complexes, indicating that chemical substances interacting with the active site do not cause major conformational changes. The lead molecule's protein-ligand complex had an RMSD value of 1 nm **(Figure 8)**. The RMSF analysis revealed minimal variation in amino acid residues, with the loop area showing stability, as depicted in **(Figure 8)**.

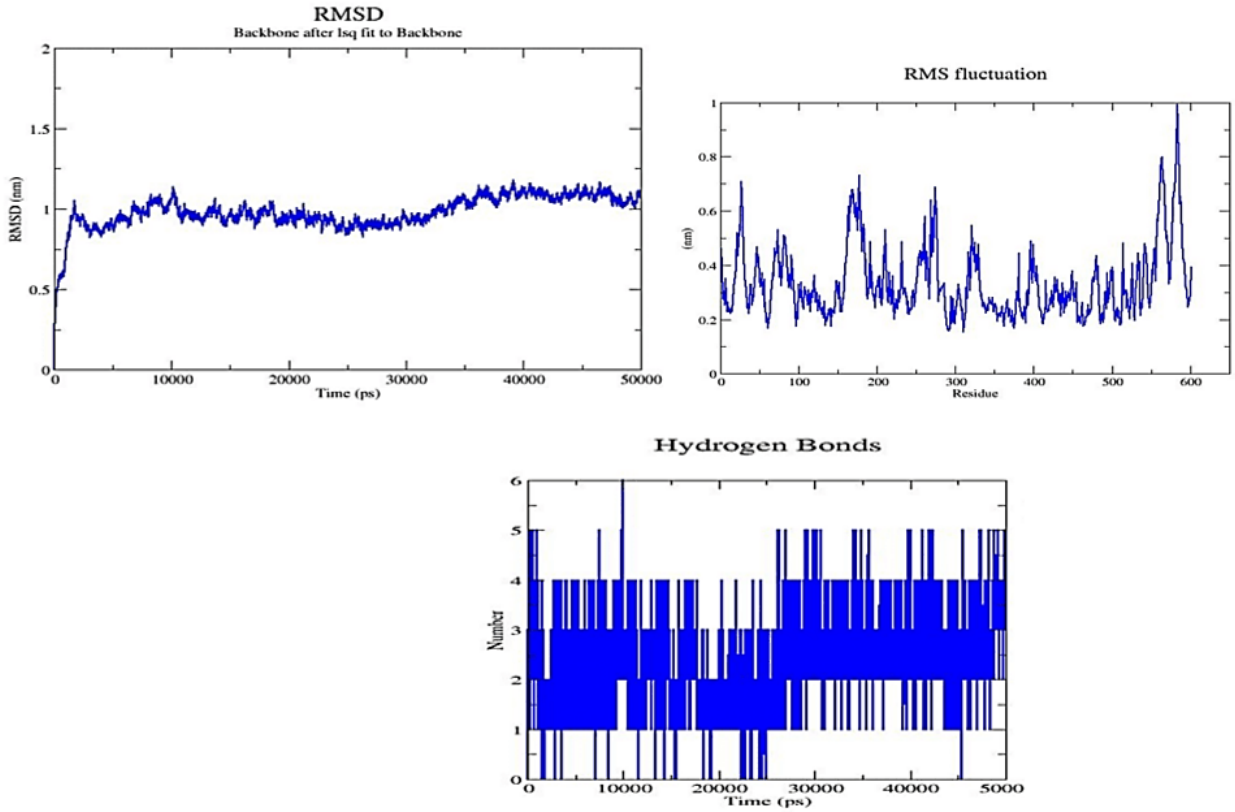

Figure 8: RMSD backbone of Cot H3- Lead Fig 11: RMSD, RMSF, and H-bond interaction between Cot H3- lead complexes

3.12. DFT calculation

The electronic properties of the lead molecule were analysed using frontier orbital energies, specifically the lowest unoccupied molecular orbital (LUMO) and highest occupied molecular orbital (HOMO). LUMO indicates electron affinity, while HOMO reflects ionization potential. The energy gap between HOMO and LUMO determines the molecule's chemical stability and reactivity. A lower gap suggests higher reactivity, instability, and polarizability. DFT calculations revealed HOMO and LUMO values ranging from -0.23 to -0.106 eV, with the energy difference between them at -0.129 eV.[40] (**Figure 9 and Table 8**).

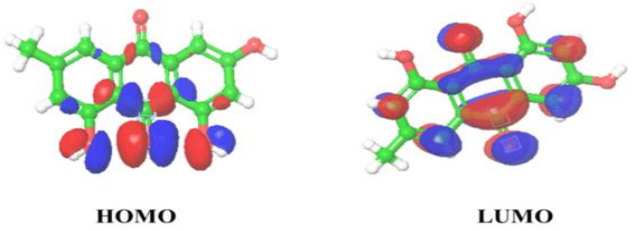

Figure 9: HOMO and LUMO profile of the lead molecule

Table 8: HOMO and LUMO values of the lead molecule

S. No	Compound	HOMO (eV)	LUMO (eV)	HOMO-LUMO Gap (eV)
1	3220	-0.23	-0.106	-0.129

4. Discussion

This study highlights the potential of emodin as a promising lead compound for treating mucormycosis, a severe fungal infection primarily caused by *Rhizopus* species. The focus was on COT H3, a vital virulence factor that enables *Rhizopus* to evade the host immune system. Targeting virulence factors like COT H3, instead of essential metabolic pathways, reduces the risk of resistance while neutralizing key mechanisms of infection. COT H3 plays a crucial role in *Rhizopus* pathogenesis, aiding spore adhesion and germination, which are essential for initiating infection and interacting with host immune cells.[28] Previous research suggests that inhibiting spore coat proteins like COT H3 reduces fungal viability and virulence, making them ideal drug targets. Our in-silico analysis confirmed COT H3 as a viable target for antifungal therapy. Among the phytocompounds screened, emodin demonstrated the highest binding affinity for COT H3, with a glide score of -8.37 kcal/mol and a binding free energy of -33.735 kcal/mol, indicating a strong, stable interaction. Key residues, including Thr573, Asn571, and Ser408, were involved in the binding, suggesting emodin could effectively inhibit COT H3's function. Molecular dynamics (MD) simulations showed the emodin-COT H3 complex remained stable, with low RMSD values, indicating its potential for prolonged

inhibitory activity and reduced fungal recovery or resistance development.[15,30]

ADME (Absorption, Distribution, Metabolism, and Excretion) and toxicity predictions revealed emodin's favorable pharmacokinetic properties, such as good bioavailability, metabolic stability, and minimal toxicity.[39] These attributes suggest that emodin can achieve therapeutic concentrations without significant side effects. Its natural origin may also lower toxicity and improve patient tolerance compared to synthetic antifungals.[17] Emodin's antifungal activity against *Rhizopus* aligns with its reported efficacy against other fungal pathogens. Its targeting of COT H3 offers a novel mechanism compared to traditional antifungals like amphotericin B or azoles. When compared to FDA-approved drugs like Amphotericin B (PubChem ID: 5280965), emodin showed superior activity, reinforcing its potential as an effective therapeutic agent.[5] These in-silico results highlight emodin as a promising candidate for the development of novel antifungal therapies targeting mucormycosis. Further experimental validation is needed to confirm its efficacy and safety, and optimization could improve its potency and pharmacokinetic properties.[21,22,37,38]

5. Conclusion

Finally, finding bioactive substances that could successfully inhibit *Rhizopus arrhizus* potential targets was the goal of the current investigation. Using the Robetta server, the three-dimensional structure of the target protein Cot H3 was modeled. Molecular dynamics simulations demonstrated the structural stability and adaptability of the model. The lead compound identification was made easier by the molecular docking technique. Based on a computational toxicity assessment, the top 5 lead compounds were selected against the Cot H3 protein. The discovered lead compounds interact favorably with the Cot H3 binding site and have high Glide scores and binding affinities**.** Only one of the five lead compounds, emodin (3220), exhibited ADME characteristics that were acceptable and satisfied Lipinski's rule of five. The greatest one-lead compound's ADME properties performed better than the FDA-approved medication. Afterward, a molecular dynamics simulation was run to determine the protein and lead chemical complex's conformational flexibility and stability. DFT simulations were used to anticipate the reactive function groups on the identified lead molecule to optimise and enrich the lead further. Therefore, this putative lead compound seems to be a bioactive molecule that can overcome Cot H3's pathogenicity in *Rhizopus arrhizus.*

6. Source of Funding

This work is supported by the Alagappa University Research Fund (AURF) Seed Money 2024 [grant sanctioned vide Letter No. AU/SO(P&D)/AURF Seed Money/2024 Alagappa University, Karaikudi, Tamil Nadu, India, Date 11th December 2024], DST-FIST [SR/ FST/LSI-667/2016(C)], DST-PURSE [SR/PURSE Phase 2/38 (G)], UGC- Innovative and MHRD-RUSA- phase 2.0 grant sanctioned vide [F.24-51/2014-U policy (TNMulti – Gen), Dept of Edn. Govt of India Dt, 09.10.2018] for the infrastructure facilities available in the Department of Bioinformatics, Alagappa University.

7. Conflict of Interest

None.

References

1. Abel R, Ramos MP, Chen Q, Pérez-Sánchez H, Coluzzi F, Rocco M, et al. Computational Prediction of Potential Inhibitors of the Main Protease of SARS-CoV-2. *Front Chem.* 2020;8:590263.
2. Hassan AS, Elfiky AA, Elgohary AM. Triple in silico targeting of IMPDH enzyme and RNA-dependent RNA polymerase of both SARS-CoV-2 and Rhizopus oryzae. *Future Microbiol*. 2024;19:9–19.
3. Agrawal R, Yeldandi A, Savas H, Parekh ND, Lombardi PJ, Hart EM. Pulmonary mucormycosis: Risk factors, radiologic findings, and pathologic correlation. *Radiographics.* 2020;40(3):656–66.
4. Amala M, Rajamanikandan S, Prabhu D, Surekha K, Jeyakanthan J. Identification of anti-filarial leads against aspartate semialdehyde dehydrogenase of *Wolbachia* endosymbiont of *Brugia malayi*: Combined molecular docking and molecular dynamics approaches. *J Biomol Struct Dyn.* 2019;37(2):394–410
5. Anderson RJ, Weng Z, Campbell RK, Jiang X. Main-chain conformational tendencies of amino acids. *Proteins.* 2005;60(4):679–89.
6. Andrade JC, Dos Santos ATL, Da Silva ARP, Freitas MA, Afzal MI, Gonçalo MIP, et al. Phytochemical characterization of the *Ziziphus joazeiro* Mart. metabolites by UPLC-QTOF and antifungal activity evaluation. *Cell Mol Biol (Noisy-le-grand).* 2020;66(4):127–32.
7. Singh A, Varadarajan A, Pant P, Singh TP, Vikram NK, Sharma S, et al. Identification of potential anti-mucor agents by targeting endothelial cell receptor glucose-regulated protein-78 using in silico approach. *J Biomol Struct Dyn*. 2024;42(8):4344–55
8. Avasthi A, Jain S, Bhatnagar M, Ghosal S. In vitro antibacterial, antifungal, antioxidant, and antihemolytic activities of *Alpinia galanga*. *Int J Pharm Bio Sci.* 2015;7(1):78–89.
9. Balajee SA, Borman AM, Brandt ME, Cano J, Cuenca-Estrella M, Dannaoui E, et al. Sequence-based identification of *Aspergillus*, *Fusarium*, and *Mucorales* species in the clinical mycology laboratory: Where are we and where should we go from here? *J Clin Microbiol*. 2009;47(4):877–84.
10. Bhandari J, Thada PK, Nagalli S. Rhinocerebral mucormycosis. In: StatPearls [Internet]. Treasure Island (FL): StatPearls Publishing; 2022 [updated 2021 Nov 25]. Available from: https://www.ncbi.nlm.nih.gov/books/NBK559288/ [accessed 28 June 2025].
11. Dalal V, Dhankhar P, Singh V, Rakhaminov G, Golemi-Kotra D, Kumar P. Structure-Based Identification of Potential Drugs Against FmtA of Staphylococcus aureus: Virtual Screening, Molecular Dynamics, MM-GBSA, and QM/MM. *Protein J*. 2021;40(2):148–65.
12. Prabhu D, Rajamanikandan S, Sureshan M, Jeyakanthan J, Saraboji K. Modelling studies reveal the importance of the C-terminal inter motif loop of NSP1 as a promising target site for drug discovery and screening of potential phytochemicals to combat SARS-CoV-2. *J Mol Graph Model.* 2021;106:107920.
13. Dubey P, Sett R. Antifungal properties of seeds Cassia tora Linn. *Horticult Int J.* 2018;2(6):299–301.
14. Elgohary AM, Elfiky AA, Barakat K. GRP78: A possible relationship of COVID-19 and the mucormycosis; in silico perspective. *Comput Biol Med*. 2021;139:104956.

15. Gebremariam T, Liu M, Luo G, Bruno V, Phan QT, Waring AJ, et al. CotH3 mediates fungal invasion of host cells during mucormycosis. *J Clin Invest*. 2014;124(1):237–50.
16. Gebremariam T, Alkhazraji S, Soliman SSM, Gu Y, Jeon HH, Zhang L, et al. Anti-CotH3 antibodies protect mice from mucormycosis by prevention of invasion and augmenting opsonophagocytosis. *Sci Adv.* 2019;5(6):eaaw1327.
17. Gurunathan S, Lee AR, Kim JH, Antifungal effect of nanoparticles against COVID-19 linked black fungus: A perspective on biomedical applications. *Int J Mol Sci.* 2022;23(20):12526.
18. Ibrahim AS, Spellberg B, Walsh TJ, Kontoyiannis DP. Pathogenesis of mucormycosis. *Clin Infect Dis.* 2012;54 Suppl 1(Suppl 1):S16–22.
19. Khan T, Dixit S, Ahmad R, Raza S, Azad I, Joshi S, et al. Molecular docking, PASS analysis, bioactivity score prediction, synthesis, characterization, and biological activity evaluation of a functionalized 2-butanone thiosemicarbazone ligand and its complexes. *J Chem Biol*. 2017;10(3):91–104.
20. Kottarathil M, Thayanidhi P, Sathyamurthy P, Kindo AJ. Rise of mucormycosis during the COVID-19 pandemic and the challenges faced. *Curr Med Mycol.* 2023 Mar;9(1):44–55.
21. Madanagopal P, Ramprabhu N, Jagadeesan R. In silico prediction and structure-based multitargeted molecular docking analysis of selected bioactive compounds against mucormycosis. *Bull Natl Res Cent.* 2022;46(1):24.
22. Madanagopal P, Muthusamy S, Pradhan SN, Prince PR. Construction and validation of a multi-epitope in silico vaccine model for lymphatic filariasis by targeting *Brugia malayi*: a reverse vaccinology approach. *Bull Natl Res Cent.* 2023;47(1):47.
23. Ferreira MRA, Santiago RR, Silva-Rocha WP, de Souza LBF, de Mello JCP, Langassner SMZ, et al. In vitro antifungal activity and phytochemical characterization of *Eugenia uniflora*, *Libidibia ferrea*, and *Psidium guajava*. *Braz J Pharm Sci.* 2020;56:e18456.
24. Mahalaxmi I, Jayaramayya K, Venkatesan D, Subramaniam MD, Renu K, Vijayakumar P, et al. Mucormycosis: An opportunistic pathogen during COVID-19. *Environ Res*. 2021;201:111643.
25. Morales-Salazar I, Garduño-Albino CE, Montes-Enríquez FP, Nava-Tapia DA, Navarro-Tito N, Herrera-Zúñiga LD, et al. Synthesis of Pyrrolo[3,4-b]pyridin-5-ones via Ugi-Zhu reaction and in vitro-in silico studies against breast carcinoma. *Pharmaceuticals (Basel).* 2023;16(11):1562.
26. Naqvi HA, Yousaf MN, Chaudhary FS, Mills L. Gastric Mucormycosis: An Infection of Fungal Invasion into the Gastric Mucosa in Immunocompromised Patients. *Case Rep Gastrointest Med.* 2020;2020:8876125.
27. Paramashivam S, Dhiraviam KN. Computational insights into the identification of a potent matrix metalloproteinase inhibitor from Indigofera aspalathoides to control cancer metastasis. *3 Biotech.* 2021;11(5):206.
28. Pradiba D, Aarthy M, Shunmugapriya V, Singh SK, Vasanthi M. Structural insights into the binding mode of flavonols with the active site of matrix metalloproteinase-9 through molecular docking and molecular dynamic simulations studies. *J Biomol Struct Dyn*. 2018;36(14):3718–39.
29. Pokharkar O, Lakshmanan H, Zyryanov G, Tsurkan M. In Silico Evaluation of Antifungal Compounds from Marine Sponges against COVID-19-Associated Mucormycosis. *Mar Drugs.* 2022;20(3):215.
30. Sahayarayan JJ, Rajan KS, Vidhyavathi R, Nachiappan M, Prabhu D, Alfarraj S, et al. *In-silico* protein-ligand docking studies against the estrogen protein of breast cancer using pharmacophore-based virtual screening approaches. *Saudi J Biol Sci*. 2021;28(1):400–7.
31. Scott WRP, Hunenberger PH, Tironi IG, Mark AE, Billeter SR, Fennen J, et al. The GROMOS biomolecular simulation program package. *J Phys Chem A.* 1999;103(19):3596–3607.
32. Schier C, Gruhlke MCH, Reucher G, Slusarenko AJ, Rink L. Combating black fungus: Using allicin as a potent antifungal agent against mucorales. *Int J Mol Sci.* 2023;24(24):17519.
33. Sharma A, Kaur I. Targeting β-glucan synthase for Mucormycosis "The 'black fungus" maiming Covid patients in India: computational insights. *J Drug Deliv Ther.* 2021;11(3 Suppl):9–14.
34. Skiada A, Petrikkos G. Cutaneous mucormycosis. *Skinmed.* 2013;11(3):155–9
35. Soltan MA, Eldeen MA, Elbassiouny N, Kamel HL, Abdelraheem KM, El-Gayyed HA, et al. In Silico designing of a multitope vaccine against rhizopus microsporus with potential activity against other mucormycosis causing fungi. *Cells.* 2021;10(11):3014.
36. Spellberg B. Gastrointestinal mucormycosis: an evolving disease. *Gastroenterol Hepatol (N Y).* 2012;8(2):140–2.
37. Suhandi C, Alfathonah SS, Hasanah AN. Potency of Xanthone Derivatives from Garcinia mangostana L. for COVID-19 treatment through angiotensin-converting enzyme 2 and main protease blockade: A computational study. *Molecules*. 2023;28(13):5187.
38. Rajamanikandan S, Soundarya S, Paramasivam A, Prabhu D, Jeyakanthan J, Ramasamy V. Computational identification of potential lead molecules targeting rho receptor of Neisseria gonorrhoeae. *J Biomol Struct Dyn*. 2022;40(14):6415–25.
39. Wang XM, Guo LC, Xue SL, Chen YB. Pulmonary mucormycosis: A case report and review of the literature. *Oncol Lett*. 2016;11(5):3049–53.
40. Zieniuk B, Ononamadu CJ, Jasińska K, Wierzchowska K, Fabiszewska A. Lipase-catalysed synthesis, antioxidant activity, antimicrobial properties and molecular docking studies of butyl dihydrocaffeate. *Molecules.* 2022;27(15):5024.

Cite this article: Sugumaran M, Viswanathan N, Thangavel K, Dhamodharan P, Ramasamy V. Structural insight into CotH3 protein inhibition targeting mucormycosis infection through computational approaches. *Indian J Microbiol Res*. 2025;12(2):266–276.